ACS APPLIED MATERIALS & INTERFACES

Research Article

www.acsami.org

Gold Nanoflower@Gelatin Core–Shell Nanoparticles Loaded with Conjugated Polymer Applied for Cellular Imaging

Qianling Cui, Fang He,* Xiaoyu Wang, Bihua Xia, and Lidong Li*

State Key Laboratory for Advanced Metals and Materials, School of Materials Science and Engineering, University of Science and Technology Beijing, Beijing 100083, China

ABSTRACT: In the present work, a facile one-pot method is designed to fabricate a core–shell fluorescent nanoparticle (NP) for cellular imaging based on a new cationic conjugated polymer, poly[9,9′-bis(6,6′-(*N*,*N*,*N*-trimethylaminium)-fluorene-2,7-ylenevinylene-co-alt-2,5-dicyano-1,4-phenylene] (PFVCN). Gold nanoflowers (AuNFs) are prepared by a seedless method, in which a gelatin layer formed through a sol–gel phase transition is deposited on the surface of each AuNF. The cationic PFVCN self-assembles onto the negative surface of the resultant (AuNF@Gelatin NPs) driven by electrostatic attraction. An obvious enhancement of fluorescence intensity is observed. The AuNF@Gelatin/PFVCN NPs exhibit excellent cytocompatibility, and their cellular imaging ability is demonstrated when cocultured with HeLa cells. AuNF@Gelatin/PFVCN hybrid NPs are expected to be a desirable material in the field of cellular imaging and biosensing.

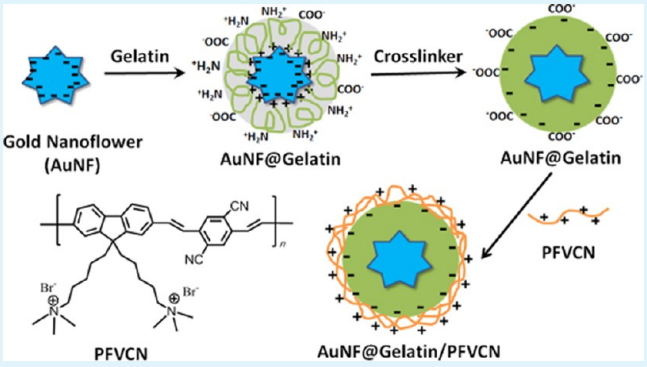

KEYWORDS: *conjugated polymers, self-assembly, core–shell nanoparticles, fluorescence, gold nanoflowers, cellular imaging*

INTRODUCTION

The application of nanotechnology to the development of safe, efficient and hydrophilic fluorescent nanoparticles (NPs) has attracted considerable research interests because of their promising application in biological labeling, sensing and imaging.[1−3] A wide range of materials such as small organic molecules, carbon nanotubes, proteins, polymers, quantum dots, graphene and carbon NPs have been used to fabricate such fluorescent NPs.[4−9] Water-soluble conjugated polymers contain π-delocalized backbones and possess many advantages, such as high absorption cross sections, amplification the fluorescence of small organic molecules and other dyes through energy transfer. For these reasons, they have emerged as a novel and promising material for sensing, imaging, diagnosis, and therapy in biological science.[10−15] Recently, various fluorescent NPs based on water-soluble conjugated polymers have been fabricated, and their potential application for bioimaging and biosensing has been demonstrated.[13] However, for the purpose of achieving practical applications for these conjugated polymers NPs in vivo, significant challenges still remain with respect to enhance the fluorescence intensity, stability and the biocompatibility.

NPs with core–shell architecture show great potential as candidate for fluorescent NPs, due to their benefits of incorporating diverse functionalities into a single hybrid nanoparticle.[16−21] In particular, core–shell NPs with a metal core have been developed, and their interaction with nearby fluorophores have been studied. Metal NPs (such as gold or silver) may quench or enhance fluorescence depending on the distance between the fluorescent dye and the metal. When the distance is suitable, an enhanced effect would be observed, namely a metal-enhanced fluorescence (MEF).[22−24] This MEF effect was used to design fluorescent NPs, in which the brightness and photostability of the fluorophores are increased. Therefore, a variety of functional fluorescent NPs with metal core have been fabricated and reported.[25−40] Our group previously reported the preparation of Ag@SiO_2 and Ag@PNIPAM core–shell NPs loaded with conjugated polymer, whose application in cellular imaging was demonstrated *in vivo*.[25,26] However, silver NPs always show poor biocompatibility, which limits their application *in vivo*. Therefore, gold NPs are generally chosen to instead of silver NPs due to their better biocompatibility.[41,42] Recently, we also developed a new kind of hybrid core–shell nanosphere by combining the in situ formation of Au nanoparticles and covalent cross-linking of biocompatible carboxymethyl starch dialdehyde (CMSD) and chitosan (CTS).[43] After assembling cationic conjugated polymer on the surface, these biocompatible hybrid nanospheres exhibited MEF effects, excellent biodegradability and good biocompatibility for cellular imaging. However, the procedure of the preparation of this hybrid system needs several steps. As a result, to prepare the systems with a simple procedure remains a big challenge for designing more efficient fluorescence NPs.

Received: November 5, 2012
Accepted: December 13, 2012
Published: December 13, 2012

Scheme 1. Synthetic Route of the Water-Soluble Conjugated Polymer PFVCN

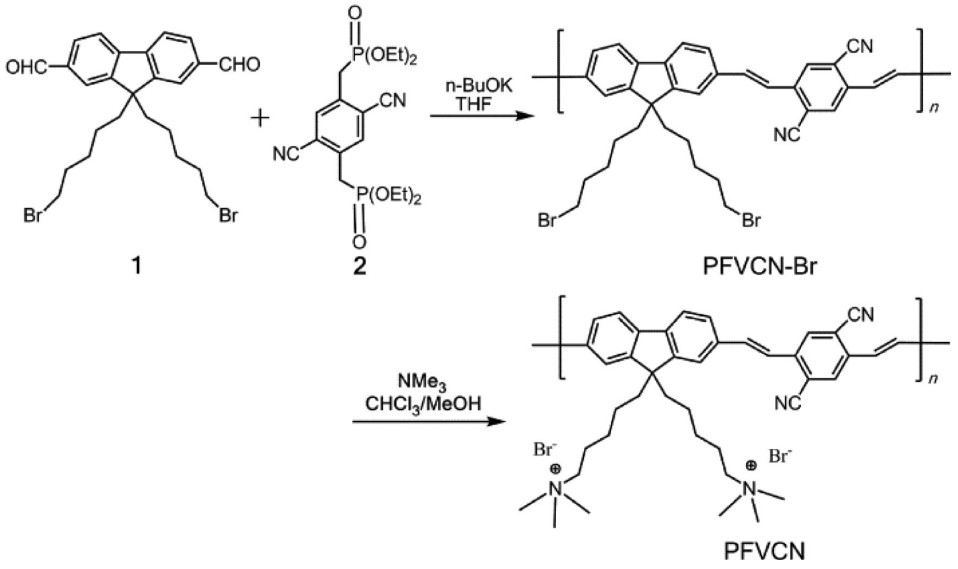

Because the emission of the fluorophore would be quenched if it was attached onto the metal NPs directly, a shell layer is needed to separate the fluorophore and the metal core. Certain kinds of materials such as silica,[25,27,29,30,33,38,44] polymers,[17,26,32] polyelectrolyte films fabricated by layer-by-layer,[11,31] and proteins,[45] have been used as the shell layer of the core−shell fluorescent NPs. However, the preparation of such NPs is complicated, and some of them display high cytotoxicity. Gelatin is a natural material that is obtained from thermally and hydrolytically denatured collagen. Gelatin has many advantages, such as excellent biocompatibility and nonimmunogenicity, and it has been applied extensively in the fields of food, pharmacy, industry, and cosmetics.[46−51] In addition, gelatin can be easily coated onto the metal NPs with surface area-to-volume ratios, through a sol−gel phase transition.[50] Therefore, we consider that gelatin represents an ideal shell layer for the fabrication of core−shell fluorescent NPs for potential application in vivo.

In this study, a unique hybrid NP with a gold nanoflower (AuNF) as the core and gelatin as the shell (AuNF@Gelatin NP) was designed and prepared by a facile one-pot method. The AuNF core was obtained by a seedless method. A single layer of gelatin was then easily formed on the core through a sol−gel phase transition and fixed by cross-linking. A new water-soluble conjugated cationic polymer, poly[9,9′-bis(6,6′-(*N,N,N*-trimethylaminium)fluorene-2,7-ylenevinylene-co-alt-2,5-dicyano-1,4-phenylene] (PFVCN), was synthesized and self-assembled onto the AuNF@Gelatin NPs. The MEF effect of hybrid system to PFVCN was controlled through tuning the thickness of gelatin shell. These fluorescent NPs were characterized by transmission electron microscopy (TEM), zeta-potential measurements, UV−vis spectroscopy, fluorescence spectroscopy, and their cytotoxicity and ability of cellular imaging were also determined.

EXPERIMENTAL SECTION

Materials. 2,7-Diformyl-9,9-di(6′-bromohexy)fluorene (1)[25] and 1,4-bis(diethylphosphinatyl methyl)-2,5-dicyanobenzene (2)[52] were prepared according to the reported procedures. Gelatin from cold water fish skin and 2-[4-(2-hydroxyethyl)-1-piperazinyl]ethanesulfonic acid (HEPES) were purchased from Sigma-Aldrich. Analytical grade chloroauric acid tetrahydrate ($HAuCl_4{\cdot}4H_2O$), glutaraldehyde, sodium borohydride ($NaBH_4$), sodium hydroxide (NaOH), hydrochloric acid (HCl), nitric acid (HNO_3), potassium *tert*-butoxide, trimethylamine, tetrahydrofuran (THF), methanol, ethanol, chloroform, and acetone were purchased from Beijing Chemical Reagent Co. Ltd. THF was purified by distillation from sodium with benzophenone. Other reagents and solvents were used as received. Ultrapure Millipore water (18.6 MΩ) was used throughout the experiments.

Synthesis of Poly[9,9′-bis(6′-(bromohexyl)fluorene-2,7-ylenevinylene-co-alt −2,5-dicyano-1,4-phenylene] (PFVCN-Br). The synthetic route was shown in Scheme 1. A solution of monomer 1 (260 mg, 0.5 mmol) and compound 2 (214 mg, 0.5 mmol) in dry THF (20 mL) was stirred at room temperature. Potassium *tert*-butoxide (224 mg, 2 mmol) was added slowly and then the solution was stirred for another 4 h at room temperature before being quenched with dilute aqueous HCl (20 mL). The solution was then poured into methanol (250 mL) under stirring. The precipitate was collected by filtration. The crude polymer was dissolved with THF and then precipitated in methanol three times and dried under vacuum to give a solid red product (100 mg, 32%). ^{1}H NMR (400 MHz, $CDCl_3$, δ): 7.85−7.69 (br, 4H), 7.58−7.49 (br, 4H), 6.74 (s, 2H), 6.58 (s, 2H), 3.26 (br, 4H), 2.04 (br, 4H), 1.63−1.58 (br, 4H), 1.18−1.08 (br, 8H), 0.65−0.54 (br, 4H); GPC: M_n = 20327, M_w = 35573, PDI = 1.75.

Synthesis of PFVCN. As shown in Scheme 1, PFVCN-Br (50 mg) was dissolved into chloroform (50 mL), and trimethylamine solution in ethanol (30%, 3 mL) was added. The mixture was stirred for 48 h at room temperature. The solvent was evaporated under vacuum and PFVCN was obtained after being dried under vacuum. ^{1}H NMR (400 MHz, DMSO-d_6, δ): 7.90−7.73 (br, 4H), 7.70−7.64 (br, 4H), 6.85 (s, 2H), 6.65 (s, 2H), 3.35 (br, 4H), 3.11−3.15 (br, 4H), 2.91−3.10 (br, 18H), 2.01−2.12 (br, 4H), 1.47 (br, 4H), 1.08 (br, 4H), 0.55−0.40 (br, 4H).

Synthesis of Gold Nanoflowers. All glasswares were cleaned with aqua regia (HCl/HNO_3 in 3:1 ratio by volume) and rinsed with ultrapure water. An aqueous stock solution of HEPES with a concentration of 100 mM was prepared, and its pH was adjusted to 7.4 ± 0.5 by adding 1 M NaOH solution. 200 μL of 100 mM HEPES was mixed with 1.8 mL of deionized water, followed by addition of 40 μL of 25 mM $HAuCl_4$ solution. Without shaking, the color of the solution changed from light yellow to colorless and finally to turbid blue at room temperature within 30 min. This AuNFs solution was used after 1 h.

Preparation of AuNF@Gelatin NPs. The obtained AuNF solution (~2 mL) was heated to 50 °C using water bath, and added by 8 mL gelatin solution (preheated at 50 °C) under vigorous stirring. The final concentration of gelatin was controlled at 1 mg mL^{-1}, 5 mg mL^{-1}, 10 mg mL^{-1}, respectively. This mixture was stirred at 50 °C for 30 min, after which its pH was adjusted to ~3.0 using 1 M HCl. Then

Scheme 2. Schematic Illustration of the Preparation of the AuNF@Gelatin/PFVCN NPs

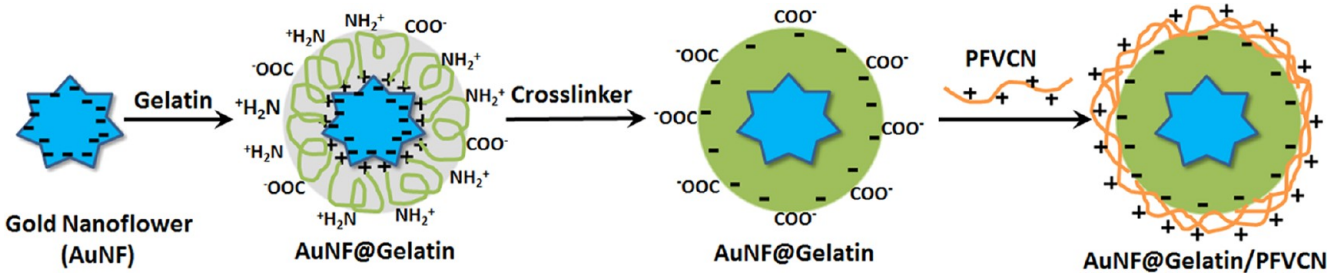

under constant stirring at 40 °C, 30 mL of acetone was dropwisely added during 15 min. 80 μL of 25% glutaraldehyde was admixed to the stirring mixture, which was further stirred at 40 °C for 1 h, followed by overnight incubation at room temperature. To eliminate the residual glutaraldehyde, a small amount of 0.1 M $NaBH_4$ solution was added into the mixture, and stirred for another 2 h. The NPs were then collected by centrifugation, washed with water twice, and finally dispersed in 0.5 mL of H_2O.

Preparation of AuNF@Gelatin/PFVCN NPs. Briefly, 100 μL of the prepared AuNF@Gelatin NPs solution was mixed with 20 μL of 1 mM PFVCN solution and incubated for 30 min. Then, the formed AuNF@Gelatin/PFVCN samples were centrifuged, washed with water, and dispersed into 100 μL of water. Supernatant solution containing free PFVCN was removed and diluted for UV−vis measurement. The absorbance of the supernatant was compared with that before absorption to calculate the absorption efficiency, which was about 30%. For the metal-enhanced fluorescence measurements, 6 μL of 0.1 mM PFVCN was added into 1 mL of 10 mM PBS solution (pH 7.4), followed by the addition of 20 μL of AuNF@Gelatin NPs, and its fluorescence spectra were recorded after 30 min. The enhancement factor was calculated by comparing the fluorescence intensity before and after introduction of AuNF@Gelatin NPs.

Cytotoxicity Assay by MTT Method. The cytotoxicity of the NPs was studied using a 3-(4,5-dimethylthiazol-2-yl)-2,5-diphenyltetrazolium bromide (MTT) cell-viability assay. HeLa cervical carcinoma cells were seeded into 96-well plates at an intensity of 7×10^4 cells mL^{-1} in DMEM medium and maintained for 24 h at 37 °C in a humidified environment containing 5% CO_2. Different amounts of AuNF@Gelatin/PFVCN nanospheres solutions (0.5 μL, 1.0 μL, 2.0 μL, 3.0 μL, 4.0 μL, 5.0 μL) were then added into the medium, and the cells were cultured for another 24 h. After pouring out the medium, 100 μL of freshly prepared MTT (1 mg mL^{-1} in PBS) was added to each well and incubated for 4 h. After removing the MTT medium solution, the cells were lysed by adding 100 μL of DMSO. The plate was gently shaken for 5 min, and then the absorbance of purple formazan at 520 nm was monitored using a Spectra MAX 340PC plate reader. To provide a comparative study of the toxicity of nanospheres to the cells, AuNF@Gelatin NPs and PFVCN solution were also added separately instead of the AuNF@Gelatin/PFVCN NPs to incubate with the cells in the MTT experiment. The amount of NPs and PFVCN solution used was the same as that in the AuNF@Gelatin/PFVCN NPs.

Cellular Imaging Experiments. Ten microliters of AuNF@Gelatin/PFVCN NPs was added into 1 mL of DMEM medium containing HeLa cells in a 35 × 35 mm plate ([PFVCN] = 5.88×10^{-7} M). The plate was then incubated for 10 h at 37 °C in a humidified environment containing 5% CO_2. Then, fluorescence images and phase contrast bright-field images were recorded on a fluorescence microscope (Olympus IX71) without further treatment using a 455/70 nm excitation filter with 500 ms exposure time.

Instrumentation. ^1H NMR spectra were recorded on 400 MHz AC Bruker spectrometers. Gel permeation chromatography (GPC) analysis was carried out on a Waters Styragel system using polystyrene as the calibration standard and THF as eluent. The zeta-potential measurements of the nanocomposites were measured using a Nano ZS90 Zetasizer (Malvern Instruments Ltd., UK). The TEM images were recorded by a JEM 2100 transmission electron microscope with an accelerating voltage of 200 kV. The samples were stained with phosphotungstic acid. The UV−vis extinction/absorption spectra were measured on a Hitachi U3900 spectrophotometer. Fluorescence spectra of the samples were obtained by a Hitachi F-7000 spectrometer. The fluorescence quantum yield of the sample was measured using fluorescein in 0.1 M NaOH as the standard. Cellular images were taken with the fluorescence microscope using a 100 W mercury lamp as the light source.

RESULTS AND DISCUSSION

Synthesis and Characterization of AuNF@Gelatin/PFVCN NPs. The preparation of the AuNF@Gelatin/PFVCN hybrid fluorescent NPs is schematically illustrated in Scheme 2. Herein, AuNFs were selected as the core material for two reasons. First, it has been demonstrated through experiment and theory that anisotropic metal NPs display stronger MEF behavior, because of the enhanced local electric field close to the tips of the particles.[53,54] Second, AuNF was easily prepared according to the method of Xie, using HEPES as both the reducing and stabilizing agent.[55] Compared with other gold NPs obtained via the seeded growth method capped with toxic surfactant, the HEPES coating on the gold NPs provides a relatively "clean" surface, which is easily post-modified for biological applications.

The TEM images of the obtained AuNFs using Xie's method are shown in Figure 1. The flowerlike gold NPs have several tips and a rough surface, which may facilitate the MEF effect. Since the size of metal NPs is another factor of MEF, here we have chosen to use the NPs with a diameter of 70−90 nm, considering the appropriate ratio of absorption and scattering

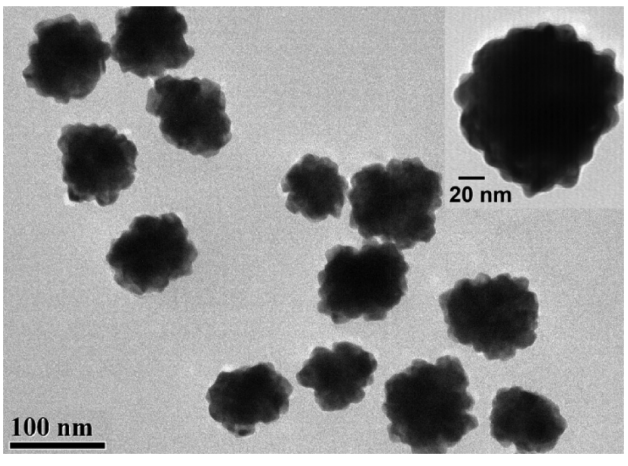

Figure 1. TEM image of synthesized gold nanoflowers (AuNFs). The inset is the magnified TEM image of the AuNFs.

dx.doi.org/10.1021/am302589g | ACS Appl. Mater. Interfaces 2013, 5, 213−219

cross section and their ability to enter cells after modification.[35,56] The average diameter of the obtained AuNFs is about 88 nm, as shown in Figure 1. Figure 2a shows the zeta-potential

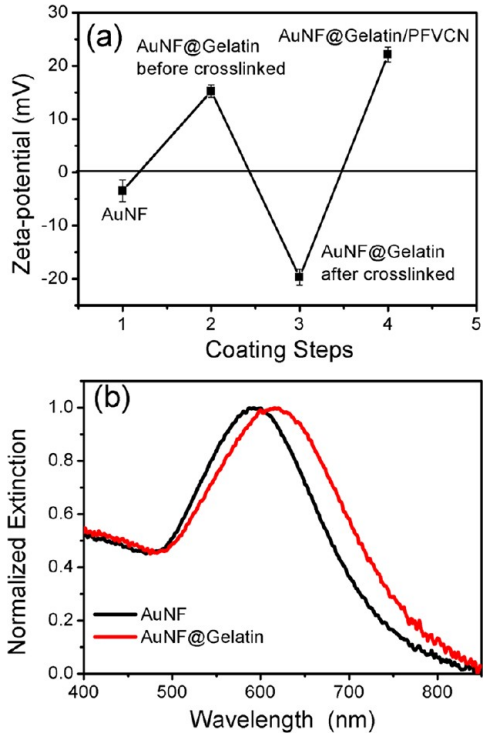

Figure 2. (a) Zeta-potential values of the AuNFs, before and after cross-linking of AuNF@Gelatin, AuNF@Gelatin/PFVCN NPs; (b) extinction spectra of the AuNFs and AuNF@Gelatin NPs, taking AuNF@Gelatin-2 as an example.

values of each NP in the coating steps. The value for the AuNF was determined as about −3.5 mV. They displayed a negative charge in aqueous solution, because of the capping agent HEPES bearing sulfonic group. The low charge density on the AuNF surface illustrated that there was few HEPES molecules present in the bulk solution. This is in favor to the self-assembly of the polyelectrolyte, because small multivalent ions in solution (e.g., citrate ions) would lead to the aggregation and flocculation of the oppositely charged polymers.[50,57,58] Moreover, without the presence of other chemicals, this AuNFs solution can be used for the followed shell built-up without further purification.

Gelatin was selected here as the shell material, on the basis that it could be easily manipulated by a sol−gel phase transition. It was known that at elevated temperature (>35 °C), the gelatin is soluble in water in coil conformation due to the formation of hydrogen-bonding with water. When the temperature decreases below 35 °C, the gelatin chains would link each other and form aggregates, resulting from stronger intramolecular hydrogen bonding between the hydroxy groups.[59] In the present work, the isoelectric point of the gelatin from cold water fish skin is ∼9.0, which is positive in neutral solution when the temperature is about 50 °C. Driven by the electrostatic attraction, the gelatin chains adsorbed onto the surface of the AuNF particles. As the temperature decreased, the gelatin aggregated on the surface of the metal particles and formed a single hydrophilic layer. The zeta-potential value of the formed AuNF@Gelatin NP is about 15 mV, arising from the presence of abundant amino groups on the gelatin shell surface. The positive charge also demonstrated the successful coating of the metal particles with the gelatin layer. The thickness of the gelatin layer was controlled by the original concentration of gelatin used. In this work, concentrations of 1, 5, and 10 mg mL^{-1} of gelatin were used to adjust the thickness of the shell, and the obtained NPs were denoted as AuNF@Gelatin-1, AuNF@Gelatin-2, and AuNF@Gelatin-3, respectively.

Because the gelatin has a sol−gel transition temperature of about 35 °C, it would be dissolved at body temperature. Therefore, glutaraldehyde was selected to cross-link the gelatin shell to make the nanostructure more stable *in vivo*. Before the addition of a cross-linker, the pH of the AuNF@Gelatin solution was adjusted to ∼3.0. Higher or lower pH would lead to instability in the mixture, and the NPs would flocculate and precipitate in the process of cross-linking. This observation is in good agreement with the reported literature.[49] After reaction for 24 h, the remaining harmful glutaraldehyde in the mixture was removed from the solution by the addition of a small amount of $NaBH_4$ solution and subsequent centrifugation. Therefore, the low toxicity of the system could be maintained. Zeta-potential experiments (Figure 2a) proved that the cross-linked AuNF@Gelatin NPs possessed a negative charge of about −20 mV. This could be explained by the fact that most of the amino groups of the gelatin (from arginine and lysine) had reacted with the glutaraldehyde, such that carboxylic acid groups were left (from aspartic acid and glutamic acid).[51,60] This negative surface is also favorable for the next coating of a positive conjugated polymer.

The extinction spectra of the AuNFs and AuNF@Gelatin NPs in water are shown in Figure 2b. The surface plasmon resonance of AuNFs is located at 592 nm. After being coated one layer of cross-linked gelatin, the maximum absorption peak of AuNF@Gelatin shifted to 616 nm. As the extinction spectra of the three obtained AuNF@Gelatin NPs are almost the same, only the spectra for AuNF@Gelatin-2 is shown here as an example. It is well-known that the SPR of metal NPs depends on the dielectric properties of the surrounding medium.[61,62] There was a red shift of 24 nm in the maximum absorption peak because of an increase in the local refractive index of the surrounding medium (1.33 of H_2O to 1.53 of gelatin).[50,61] This red-shift phenomenon also demonstrated the formation of the shell layer on the AuNFs.

To further demonstrate the core−shell structure of the AuNF@Gelatin, the morphologies of these NPs were determined by TEM, as shown in Figure 3. It can be seen that all the particles possessed a clear core−shell structure, and the thickness of the outer shell increased as the concentration of gelatin used increased. The TEM images show the average thickness of the gelatin shell of AuNF@Gelatin-1, AuNF@Gelatin-2, and AuNF@Gelatin-3 to be about 2, 10, and 50 nm, respectively.

The choice of fluorophore is also a critical factor for designing a fluorescent hybrid system. Our group previously reported that conjugated polymer, poly[9,9′-bis(6″-(*N*,*N*,*N*-trimethylammonium)-hexyl)fluorene-2,7-ylenevinylene-co-alt-1,4-phenylene dibromide] (PFV), showed good water-solubility, biocompatibility and brightness, making it suitable for use in cellular imaging in vivo.[25] The emission peak of PFV is located at 485 nm, while the AuNFs had a surface plasmon resonance at about 592 nm. There was almost no overlap between them. However, it is believed that the maximal MEF

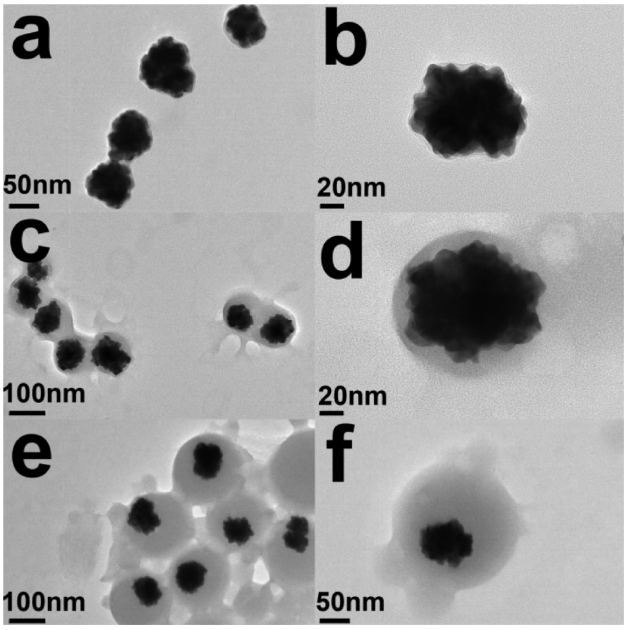

Figure 3. TEM and magnified TEM images of the obtained AuNF@Gelatin NPs with different shell thickness. (a, b) AuNF@Gelatin-1; (c, d) AuNF@Gelatin-2; (e, f) AuNF@Gelatin-3.

effect would occur if the absorption or emission peak overlaps with the surface plasmon resonance of the metal NPs.[56,63] On the basis of the above considerations, we introduced two cyano groups onto the backbone of PFV to shift its absorption and emission toward longer wavelength. The synthesis route of the conjugated polymer PFVCN is shown in Scheme 1. Figure 4

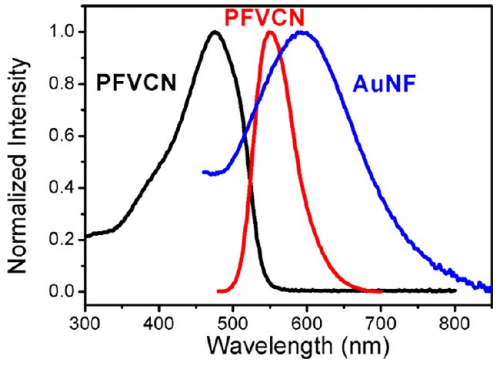

Figure 4. Normalized absorption (black) and fluorescence (red) spectra of PFVCN in water upon excitation at 470 nm, and normalized extinction spectra (blue) of AuNFs.

shows the UV–vis absorption and fluorescence emission spectra of PFVCN in water. The fluorescence maximum of PFVCN is observed at 550 nm using an excitation wavelength of 470 nm. As expected, the emission of PFVCN had a red shift (about 65 nm) compared with PFV. The fluorescence quantum yield of the PFVCN was 12.2% in water, indicating its luminous efficiency was higher than of PFV.[18] More importantly, the emission peak had a quite large overlap with the AuNFs, as shown in Figure 4.

The water-soluble conjugated polymer PFVCN was then self-assembled onto the surface of the AuNF@Gelatin NPs to obtain fluorescent NPs using electrostatic attraction as the driving force. After binding the cationic PFVCN, the zeta-potential of the AuNF@Gelatin NPs transferred from −20 to 22 mV (Figure 2a), indicating that the macromolecular dye was successfully loaded onto the negatively charged AuNF@Gelatin NPs surfaces. The strong electrostatic repulsion between these NPs ensured that they were stably dispersed in aqueous solution.

Optical Properties of AuNF@Gelatin/PFVCN NPs. Figure 5a shows the fluorescence spectra of the PFVCN (6.0

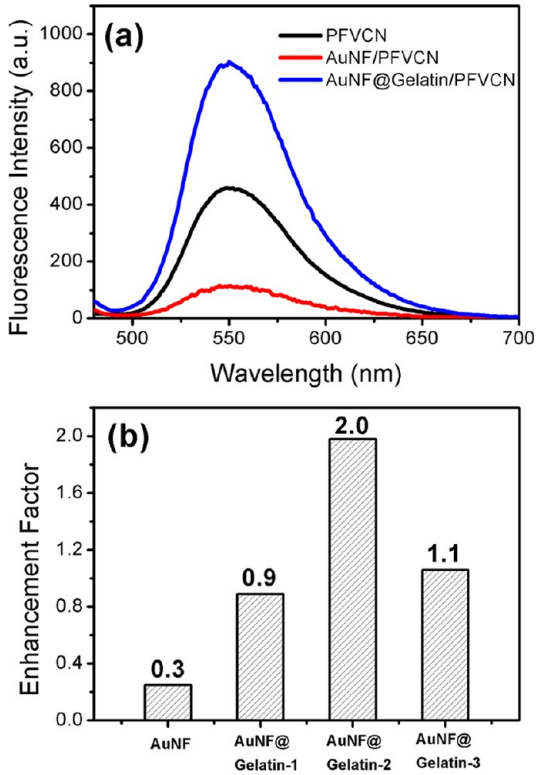

Figure 5. (a) Fluorescence spectra of PFVCN in the presence of AuNFs or AuNF@Gelatin-2 in 10 mM PBS solution (pH 7.4); (b) enhancement factor as a function of the AuNF@Gelatin NPs with different shell thickness.

$\times 10^{-7}$ M in repeat units) in the presence of AuNFs or AuNF@Gelatin-2 NPs. It was clear that the intensity of PFVCN decreased upon the addition of AuNFs, whereas it increased after the introduction of AuNF@Gelatin-2 NPs. To optimize the thickness of the gelatin shell for MEF, we determined the fluorescence enhancement factor of each AuNF@Gelatin NP with different shell thickness, and the results are shown in Figure 5b. The fluorescence enhancement factor is defined as I/I_0, where I is the emission intensity of PFVCN (6.0×10^{-7} M in repeat units) after loading 20 μL of AuNF@Gelatin NPs, and I_0 is the emission intensity of PFVCN (6.0×10^{-7} M in repeat units) in 10 mM PBS solution. The fluorescence enhancement factor for the AuNF@Gelatin NPs with gelatin shell thickness of about 0, 2, 10, and 50 nm is calculated to be 0.3, 0.9, 2.0, and 1.1, respectively. When naked AuNFs were added into the PFVCN solution, 70% of the fluorescence intensity was quenched as a result of the energy and charge transfer between the gold and PFVCN directly attached onto its surface. For the AuNF@Gelatin-1, the fluorescence emission intensity of PFVCN exhibited a small decline due to its close distance from the gold surface. When the thickness of the gelatin layer increased, the MEF effect exceeded the quenching effect. An

enhancement factor of 2.0 was observed for AuNF@Gelatin-2 with a distance of about 10 nm. When the distance increased beyond the interaction region, the addition of NPs would have no effect on the fluorescence intensity of PFVCN, like AuNF@Gelatin-3. For the following experiments of cytotoxicity and cellular imaging, AuNF@Gelatin-2/PFVCN NPs were used because of their relatively bright fluorescence.

AuNF@Gelatin/PFVCN NPs for Cellular Imaging Assay. Because the materials used here to construct the hybrid nanocomposite are of low cytotoxicity, the obtained AuNF@Gelatin/PFVCN NPs are believed to be biocompatible. Furthermore, the cationic surface and suitable size of the AuNF@Gelatin/PFVCN NPs enabled them to be easily captured by the cells. Before the application of AuNF@Gelatin/PFVCN NPs in vivo, the cytotoxicity of the PFVCN, AuNF@Gelatin and AuNF@Gelatin/PFVCN NPs were evaluated using an MTT viability assay of the HeLa cells after incubation with the NPs at different amounts for 24 h. The absorbance of MTT at 520 nm is dependent on the degree of activation of the cells. The cell viability was defined as the ratio of absorbance of the cells incubated with the samples to that of the cells incubated with culture medium only. The results of the concentration-dependent cell viability are shown in Figure 6. Pure PFVCN polymer showed a high cell viability

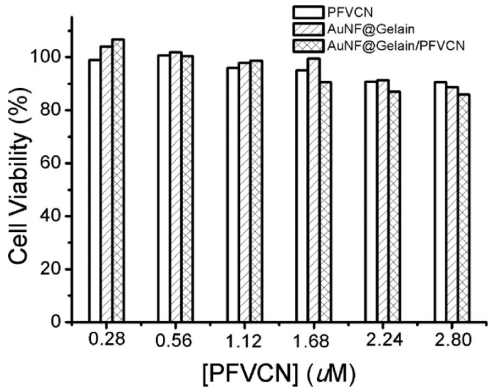

Figure 6. Cell viability results after incubation of HeLa cells with various concentrations of PFVCN (0.28–2.80 μM) adsorbed on the nanocomposite. The percentage cell viability calculated relative to that of the cells without adding NPs is defined as a viability of 100%.

(>90%) even at high concentration (2.80×10^{-6} M), proving that it was suitable for application in biological imaging. The synthesized AuNF@Gelatin NPs also displayed good cytocompatibility as expected, as did AuNF@Gelatin/PFVCN NPs. At the concentration of AuNF@Gelatin/PFVCN NPs ([PFVCN] = 5.58×10^{-7} M) used for cellular imaging in the following section, there was almost no damage to the cells. When the concentration of the nanocomposites increased up to 5-fold, the cell viability was still more than 86%.

Then, the AuNF@Gelatin/PFVCN NPs were applied for cellular imaging. Briefly, 10 μL of the NPs was added into 1 mL of a culture medium of HeLa cells (the final concentration of PFVCN was 5.58×10^{-7} M in repeat units). The fluorescence or bright-field images of the HeLa cells were monitored after cocultured with the NPs for 10 h at 37 °C, and washed twice with PBS buffer. The fluorescence image (Figure 7b) showed that the cells were stained quite well by the AuNF@Gelatin/PFVCN NPs compared with the image (Figure 7a) obtained without the presence of NPs. Figure 7d shows an overlapped

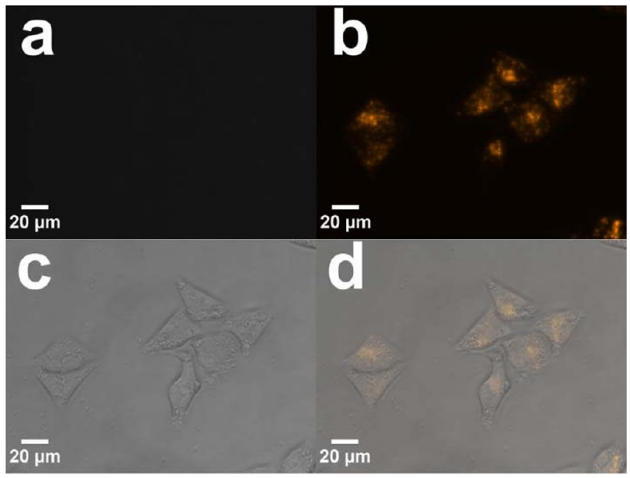

Figure 7. (a) Fluorescence image of HeLa cells without treatment of NPs; (b) fluorescence image and (c) bright-field image of HeLa cells cocultured with AuNF@Gelatin/PFVCN NPs for 10 h at 37 °C; (d) the overlapped image of b and c.

image of the fluorescence image b and the bright-field image c. It can be clearly seen that most of the NPs were observed in the cytoplasm of the HeLa cells, indicating that the AuNF@Gelatin/PFVCN NPs are favorable for fluorescent labeling and sensing in cellular environments.

CONCLUSIONS

A cationic conjugated polymer, poly[9,9′-bis(6,6′-(*N*,*N*,*N*-trimethylammonium)fluorene-2,7-ylenevinylene-co-alt-2,5-dicyano-1,4-phenylene] (PFVCN) was synthesized and its application for cellular imaging was demonstrated using AuNFs modified to exhibit enhanced fluorescence. Gelatin was first deposited onto the surface of the AuNFs through a sol–gel phase transition and then cross-linked to improve its stability. TEM images showed the AuNF@Gelatin NPs possessing a clear core–shell structure. The thickness of the gelatin layer was easily adjusted by the concentration of gelatin used, providing a convenient means to control the metal–dye distance. The emission intensity of PFVCN was enhanced about 2-fold when the gelatin layer thickness was about 10 nm. Finally, HeLa cells stained with the fluorescent NPs displayed high brightness and low cytotoxicity when AuNF@Gelatin/PFVCN NPs were applied for cellular imaging.

AUTHOR INFORMATION

Corresponding Author

*Fax: +86 10 82375712. E-mail: lidong@mater.ustb.edu.cn (L.L.); hefang@mater.ustb.edu.cn (H.F.).

Notes

The authors declare no competing financial interest.

ACKNOWLEDGMENTS

The authors gratefully acknowledge the financial support by the National Natural Science Foundation of China (20904003, 90923015), the General Financial Grant from the China Postdoctoral Science Foundation (2011M500235), the State Key Lab for Advanced Metals and Materials (2012-ZD05), the Fundamental Research Funds for the Central Universities of China (FRF-TP-09-006A, FRF-TP-09-011B) and the Program for New Century Excellent Talents in University of Ministry of Education of China (NCET-11-0576). We are grateful to Dr.

Huanxiang Yuan (Institute of Chemsitry, Chinese Academy of Sciences, China) for her kindly support for the cellular experiments. We acknowledge Dr. Xuehai Yan (Max Planck Institute of Colloids and Interfaces, Germany) for his offering gelatin and useful discussion.

REFERENCES

(1) Chan, W. C. W.; Nie., S. *Science* **1998**, *281*, 2016−2018.
(2) He, Y.; Kang, Z. H.; Li, Q. S.; Tsang, C. H. A.; Fan, C. H.; Lee, S. T. *Angew. Chem., Int. Ed.* **2009**, *48*, 128−132.
(3) Pansare, V. J.; Hejazi, S.; Faenza, W. J.; Prud'homme, R. K. *Chem. Mater.* **2012**, *24*, 812−827.
(4) Raymo, F. M. *J. Phys. Chem. Lett.* **2012**, *3*, 2379−2385.
(5) Welsher, K.; Liu, Z.; Daranciang, D.; Dai, H. *Nano Lett.* **2008**, *8*, 586−590.
(6) Shi, X.; Royant, A.; Lin, M. Z.; Agilera, T. A.; Lev-Ram, V.; Steinbach, P. A.; Tsien, R. Y. *Science* **2009**, *324*, 804−807.
(7) Bruchez, M., Jr.; Moronne, M.; Gin, P.; Weiss, S.; Alivisatos, A. P. *Science* **1998**, *281*, 2013−2016.
(8) Shen, J.; Zhu, Y.; Yang, X.; Li, C. *Chem. Commun.* **2012**, *48*, 3686−3699.
(9) Yang, S. T.; Cao, L.; Luo, P. G.; Lu, F.; Wang, X.; Wang, H.; Meziani, M. J.; Liu, Y.; Qi, G.; Sun, Y. P. *J. Am. Chem. Soc.* **2009**, *131*, 11308−11309.
(10) Thomas, S. W., III; Joly, G. D.; Swager, T. M. *Chem. Rev.* **2007**, *107*, 1339−1386.
(11) Wang, Y.; Liu, B.; Mikhailovsky, A.; Bazan, G. C. *Adv. Mater.* **2009**, *21*, 1−4.
(12) Feng, X.; Liu, L.; Wang, S.; Zhu, D. *Chem. Soc. Rev.* **2010**, *39*, 2411−2419.
(13) Zhu, C.; Liu, L.; Yang, Q.; Lv, F.; Wang, S. *Chem. Rev.* **2012**, *112*, 4687−4735.
(14) Pu, K.-Y.; Li, K.; Shi, J.; Liu, B. *Chem. Mater.* **2009**, *21*, 3816−3822.
(15) Parthasarathy, A.; Ahn, H.; Belfield, K. D.; Schanze, K. S. *ACS Appl. Mater. Interfaces* **2010**, *2*, 2744−2748.
(16) Ow, H.; Larson, D. R.; Srivastava, M.; Baird, B. A.; Webb, W. W.; Wiesner, U. *Nano Lett.* **2005**, *5*, 113−117.
(17) Wu, W.; Zhou, T.; Berliner, A.; Banerjee, P.; Zhou, S. *Chem. Mater.* **2010**, *22*, 1966−1976.
(18) Wang, X.; He, F.; Tang, F.; Ma, N.; Li, L. *Colloids Surf. A: Physicochem. Eng. Aspects* **2011**, *392*, 103−109.
(19) Zhang, R.; Wu, C.; Tong, L.; Tang, B.; Xu, Q. H. *Langmuir* **2009**, *25*, 10153−10158.
(20) Chen, Y.; Chen, H.; Zeng, D.; Tian, Y.; Chen, F.; Feng, J.; Shi, J. *ACS Nano* **2010**, *4*, 6001−6013.
(21) Ray, A.; Lee, Y. K.; Kim, G.; Kopelman, R. *Small* **2012**, *8*, 2213−2221.
(22) Wokaun, A.; Lutz, H. P.; King, A. P.; Wild, U. P.; Ernst, R. R. *J. Chem. Phys.* **1983**, *79*, 509−514.
(23) Ray, K.; Badugu, R.; Lakowicz, J. R. *J. Am. Chem. Soc.* **2006**, *128*, 8998−8999.
(24) Thomas, K. G.; Kamat, P. V. *J. Am. Chem. Soc.* **2000**, *122*, 2655−2656.
(25) Tang, F.; He, F.; Cheng, H.; Li, L. *Langmuir* **2010**, *26*, 11774−11778.
(26) Tang, F.; Ma, N.; Wang, X.; He, F.; Li, L. *J. Mater. Chem.* **2011**, *21*, 16943−16948.
(27) Aslan, K.; Wu, M.; Lakowicz, J. R.; Geddes, C. D. *J. Am. Chem. Soc.* **2007**, *129*, 1524−1525.
(28) Fu, Y.; Zhang, J.; Lakowicz, J. R. *Chem. Commun.* **2009**, 313−315.
(29) Yang, J.; Zhang, F.; Chen, Y.; Qian, S.; Hu, P.; Li, W.; Deng, Y.; Fang, Y.; Han, L.; Luqman, M.; Zhao, D. *Chem. Commun.* **2011**, *47*, 11618−11620.
(30) Li, C.; Zhu, Y.; Zhang, X.; Yang, X.; Li, C. *RSC Adv.* **2012**, *2*, 1765−1768.
(31) Liang, J.; Li, K.; Gurzadyan, G. G.; Lu, X.; Liu, B. *Langmuir* **2012**, *28*, 11302−11309.
(32) Liu, J.; Li, A.; Tang, J.; Wang, R.; Kong, N.; Davis, T. P. *Chem. Commun.* **2012**, *48*, 4680−4682.
(33) Zhang, F.; Braun, G. B.; Shi, Y.; Zhang, Y.; Sun, X.; Reich, N. O.; Zhao, D.; Stucky, G. *J. Am. Chem. Soc.* **2010**, *132*, 2850−2851.
(34) Tovmachenko, O. G.; Graf, C.; van den Heuvel, D. J.; van Blaaderen, A.; Gerritsen, H. C. *Adv. Mater.* **2006**, *18*, 91−95.
(35) Mori, K.; Kawashima, M.; Che, M.; Yamashita, H. *Angew. Chem., Int. Ed.* **2010**, *49*, 8598−8601.
(36) Bardhan, R.; Grady, N. K.; Cole, J. R.; Joshi, A.; Halas, N. J. *ACS Nano* **2009**, *3*, 744−752.
(37) Tam, F.; Goodrich, G. P.; Johnson, B. R.; Halas, N. J. *Nano Lett.* **2007**, *7*, 496−501.
(38) Cheng, D.; Xu, Q. H. *Chem. Commun.* **2007**, 248−250.
(39) Gabudean, A. M.; Focsan, M.; Astilean, S. *J. Phys. Chem. C* **2012**, *116*, 12240−12249.
(40) Cohen-Hoshen, E.; Bryant, G. W.; Pinkas, I.; Sperling, J.; Bar-Joseph, I. *Nano Lett.* **2012**, *12*, 4260−4264.
(41) Saha, K.; Agasti, S. S.; Kim, C.; Li, X.; Rotello, V. M. *Chem. Rev.* **2012**, *112*, 2739−2779.
(42) Song, S.; Qin, Y.; He, Y.; Huang, Q.; Fan, C.; Chen, H. Y. *Chem. Soc. Rev.* **2010**, *39*, 4234−4243.
(43) Xia, B.; Wang, X.; He, F.; Cui, Q.; Li, L. *ACS Appl. Mater. Interfaces* **2012**, *4*, 6332−6337.
(44) Estrada, L. C.; Roberti, M. J.; Simoncelli, S.; Levi, V.; Aramendía, P. F.; Martínez, O. E. *J. Phys. Chem. B* **2012**, *116*, 2306−2313.
(45) Aslan, K.; Leonenko, Z.; Lakowicz, J. R.; Geddes, C. D. *J. Phys. Chem. B* **2005**, *109*, 3157−3162.
(46) Liu, X.; Ma, P. X. *Biomaterials* **2009**, *30*, 4094−4103.
(47) Oh, J. K.; Drumright, R.; Siegwart, D. J.; Matyjaszewski, K. *Prog. Polym. Sci.* **2008**, *33*, 448−477.
(48) Zhang, J.; Gu, M.; Zheng, T.; Zhu, J. *Anal. Chem.* **2009**, *81*, 6641−6648.
(49) Shutava, T. G.; Balkundi, S. S.; Vangala, P.; Steffan, J. J.; Bigelow, R. L.; Cardelli, J. A.; O'Neal, D. P.; Lvov, Y. M. *ACS Nano* **2009**, *3*, 1877−1885.
(50) Liu, S.; Zhang, Z.; Han, M. Y. *Adv. Mater.* **2005**, *17*, 1862−1866.
(51) Wang, A.; Cui, Y.; Li, J.; van Hest, J. C. M. *Adv. Funct. Mater.* **2012**, *22*, 2673−2681.
(52) Wenseleers, W.; Stellacci, F.; Meyer-Friedrichsen, T.; Mangel, T.; Bauer, C. A.; Pond, S. J. K.; Marder, S. R.; Perry, J. W. *J. Phys. Chem. B* **2002**, *106*, 6853−6863.
(53) Nehl, C. L.; Liao, H. W.; Hafner, J. H. *Nano Lett.* **2006**, *6*, 683−688.
(54) Hao, F.; Nehl, C. L.; Hafner, J. H.; Nordlander, P. *Nano Lett.* **2007**, *7*, 729−732.
(55) Xie, J.; Zhang, Q.; Lee, J.; Wang, D. I. C. *ACS Nano* **2008**, *2*, 2473−2480.
(56) Ming, T.; Chen, H.; Jiang, R.; Li, Q.; Wang, J. *J. Phys. Chem. Lett.* **2012**, *3*, 191−202.
(57) Mckenna, B. J.; Birkedal, H.; Bartl, M. H.; Deming, T. J.; Stucky, G. D. *Angew. Chem., Int. Ed.* **2004**, *43*, 5652−5655.
(58) Murthy, V. S.; Cha, J. N.; Stucky, G. D.; Wong, M. S. *J. Am. Chem. Soc.* **2004**, *126*, 5292−5299.
(59) Holmgren, S. K.; Taylor, K. M.; Bretscher, L. E.; Raines, R. T. *Nature* **1998**, *392*, 666−667.
(60) Vlierberghe, S. V.; Dubruel, P.; Schacht, E. *Biomacromolecules* **2011**, *12*, 1387−1408.
(61) Liz-Marzán, L. M.; Giersig, M.; Mulvaney, P. *Langmuir* **1996**, *12*, 4329−4335.
(62) Schmitt, J.; Mächtle, P.; Eck, D.; Möhwald, H.; Helm, C. A. *Langmuir* **1999**, *15*, 3256−3266.
(63) Chen, Y.; Munechika, K.; Ginger, D. S. *Nano Lett.* **2007**, *7*, 690−696.